HHS Public Access

Author manuscript

Dev Dyn. Author manuscript; available in PMC 2019 January 01.

Published in final edited form as:

Dev Dyn. 2018 January ; 247(1): 185–193. doi:10.1002/dvdy.24601.

Characterization of Calbindin D28k Expressing Interneurons in the Ventral Horn of the Mouse Spinal Cord

Taylor L. Floyd[1], **Yiyun Dai**[1], and **David R. Ladle**[1,*]

[1]Department of Neuroscience, Cell Biology, and Physiology, Wright State University, Dayton, Ohio, United States of America

Abstract

Background—Expression of the calcium binding protein, calbindin (CB), is well established as a hallmark of Renshaw cells, a class of interneurons found in spatially restricted areas in the ventral spinal cord that directly modulate motor neuron activity. Calbindin expression, however, is not restricted only to Renshaw cells in the ventral horn, and within this population other interneuron subtypes may be identifiable on the basis of cell position and the potential for coexpression of other calcium binding proteins.

Results—Here we have quantified the changing CB expression pattern in the ventral spinal cord across postnatal development in the mouse. Fewer neurons express CB as postnatal development progresses, and those neurons frequently coexpress other calcium binding proteins (calretinin and parvalbumin) in subpopulations with distinct spatial distributions. We also found a significant portion of CB-expressing interneurons receive putative synaptic contacts from primary sensory afferents.

Conclusions—These findings suggest CB labels a heterogeneous group of interneurons in the ventral horn, some of which may process sensory information. Based on cellular position, CB expression may be a shared feature of subsets of interneurons arising from multiple ventral progenitor domains.

Keywords

calretinin; parvalbumin; postnatal; calcium binding proteins

Introduction

Descriptions of the spatial arrangement of neurons within the central nervous system provide a framework for studies that may determine how identified neurons are arranged in functional circuits. Categorizing and identifying cell types in the spinal cord has produced important tools for understanding how spinal neurons are interconnected and related through developmental lineages (Lu et al., 2015). This approach has been particularly useful in identifying the cellular components of the multiple networks in the ventral spinal cord that

*Corresponding Author: David R. Ladle, Wright State University, 3640 Colonel Glenn Highway, Dayton, OH 45435, Phone: 937-775-4692, Fax: 937-775-3391, david.ladle@wright.edu.

are directly involved in the control of motor neurons, and ultimately, locomotion in mammals (Kiehn, 2016).

Similarities in cell size, neuronal density, and other cytoarchitectural features were first used to delineate distinct laminae in the transverse plane of the spinal cord (Rexed, 1952). These initial descriptions of the cat spinal cord have been applied with minor modifications to other species (Watson et al., 2009). Identifying subsets of neurons within laminae on the basis of differential gene expression patterns provides additional insight. Shared gene expression profiles define groups of neurons that arise from the same developmental lineages or which employ similar biochemical mechanisms for function. Nevertheless, neuronal populations unified by expression of the same biomarkers likely include subgroups that differ significantly in intrinsic properties and circuit connectivity (Bikoff et al., 2016).

The expression patterns of calcium binding proteins (CBPs) in interneurons of the spinal cord illustrate this point. Calbindin D28k (CB), calretinin (CR), and parvalbumin (PV) are the three major calcium buffering proteins in neurons and descriptions of the expression patterns of each have been reported in varying detail (Andressen et al., 1993; Anelli and Heckman, 2005; Brini et al., 2014; Schwaller, 2010; Siembab et al., 2010; Zhang et al., 1990). Of these, CB has attracted particular attention due to expression that persists throughout adulthood in Renshaw cells, a functionally defined ventral horn interneuron population that mediates recurrent inhibition of motor neurons (Alvarez and Fyffe, 2007; Arvidsson et al., 1992; Carr et al., 1998). Renshaw cells cluster along the ventral gray-white matter border of the spinal cord in laminae VII and VIII (Alvarez et al., 2005; Fyffe, 1990; Thomas and Wilson, 1965). CB expression, however, is not only restricted to Renshaw cells, and CB-expressing neurons have been described in all laminae of the spinal cord, except lamina IX, which contains motor neurons. While widespread, CB expression is not homogenous, as some laminae contain higher fractions of neurons expressing CB, such as the laminae of the dorsal horn (laminae I – III) (Anelli and Heckman, 2005).

Within other regions of lamina VII in the ventral spinal cord, CB-expressing interneurons reside more dorsally and have been considered to be non-Renshaw cells (Benito-Gonzalez and Alvarez, 2012). These interneurons may belong to currently unknown, but functionally related, subpopulations. In order to more completely characterize the cellular distribution of CB in the ventral spinal cord, this study analyzed CB expression among all neurons in the ventral spinal cord across postnatal development, together with potential coexpression of other calcium binding proteins (calretinin and parvalbumin). The percentage of the CB-expressing population receiving putative contacts from primary sensory afferents, a broadly distinguishing criterion for motor function-related circuits, was also examined to produce a more comprehensive profile of CB expression among neurons in the ventral horn.

Results

To assess the density and distribution of calbindin (CB) in the ventral horn of the spinal cord (defined here as the region ventral to the central canal), CB expression in neurons of the lumbar spinal cord was characterized using immunohistochemistry during the first four weeks of postnatal development at four time points (P0, P7, P14, P28; see Fig. 1A–D for

representative images). The number of CB-expressing neurons was quantified in five animals at each stage and the six lumbar (L) segments were divided into three domains (L1 and L2, L3 and L4, L5 and L6). Numbers of CB-expressing neurons were measured in every fourth serial section throughout the entire length of the lumbar cord. The total number of CB-expressing neurons would be approximately four-fold larger than our estimates. Considering the lumbar cord as a whole, and combining cell counts in all domains together, the average number of CB-expressing neurons decreases more than 5-fold during the time course analyzed (P0: 441.2 ± 96.5 neurons per animal, n = 5 animals; P28: 82.0 ± 9.0, n = 5 animals; $F(3,19) = 9.11$, $P = 0.001$). This overall decrease is evident in the expression pattern within each lumbar domain (Fig. 1E; L1/L2: $F(3,19) = 9.871$, $P = 0.001$; L3/L4: $F(3,19) = 9.308$, $P = 0.001$; L5/L6: $F(3,19) = 5.876$, $P = 0.007$). Pairwise comparisons using Tukey's HSD test, showed significant differences in the number of CB-expressing cells at both P14 and P28 for the L1/L2 and L3/L4 domains, when compared to the initial numbers observed at P0 (L1/L2: P0, 152.0 ± 29.6; P14, 57.0 ± 8.9; P28, 29.0 ± 4.4; $P = 0.012$ at P14 and $P = 0.001$ at P28; L3/L4: P0, 144.0 ± 27.5; P14, 71.0 ± 8.7; P28, 32.0 ± 3.5; $P = 0.019$ at P14 and $P = 0.001$ at P28). Decreased expression in the caudal-most domain (L5/L6) was only significant at P28, but the decreasing trend in expression is evident also at P14 (L5/L6: P0, 145.2 ± 44.9; P28, 21.0 ± 4.8; $P = 0.015$ at P28, Tukey's HSD test). No significant differences in CB expression were found at P7 for any of the lumbar domains, suggesting the largest postnatal decrease in CB expression occurs between P7 and P14.

Calbindin is one of three primary calcium binding proteins (CBPs), and other studies have demonstrated spinal interneurons may coexpress multiple CBPs (Alvarez et al., 2005). We investigated the frequency with which CB was coexpressed with parvalbumin and/or calretinin during postnatal development. Examples of all combinations of coexpression (CB +PV, CB+CR, CB+CR+PV) were observed in the ventral lumbar cord, and representative images are shown in Figure 2. Parvalbumin immunoreactivity is abundant in the ventral spinal cord at P0, but at this time point is confined to the axons of proprioceptive sensory neurons (Arber et al., 2000; Siembab et al., 2010). PV was not detected in neurons until P7, when a fraction of CB neurons were found to coexpress PV (9.4 ± 4.0% of CB neurons). The extent of PV coexpression in CB neurons was maximal at P14, and the majority of CB neurons were also positive for PV (60.3 ± 5.2% of CB neurons). At both the P14 and P28 time points, the percentage of CB neurons that express only CB is a minor fraction of the CB population (P14: 20.6 ± 3.0%; P28 23.7 ± 2.9%). Beginning at P14, approximately one in five CB neurons were found to coexpress both PV and CR (18.0 ± 1.8% of CB neurons). This observation was more common at P28, when nearly 40% of CB neurons were found to express all three CBPs (39.2 ± 2.6% of CB neurons). The subset of CB neurons that coexpressed only CR was consistently small, however, at all times analyzed (P0: 1.4 ± 0.4%; P7: 2.1 ± 0.4%; P14: 1.1 ± 0.6%; P28 6.2 ± 1.3% of CB neurons; n=5 for all stages).

Plotting the position of CB- and other CBP-coexpressing neurons in the transverse plane of the spinal cord illustrates changes in the distribution pattern of these neurons across postnatal development. One observation is a general pattern of progressively concentrated domains of expression in the most ventral portion of the cord with increasing age. As shown in Figure 3, CB-expressing neurons are found throughout the ventral horn at P0. As the

number of cells expressing CB decreases, most notably at P14 and P28, a greater proportion of CB neurons are clustered in the extreme ventral cord.

A second observation is that the distribution of CBP-coexpressing neurons is not uniform in the ventral spinal cord (Fig. 3 and 4). At P0, neurons expressing both CB and CR are not evenly distributed within the CB-expressing population, but are found more dorsally within the ventral horn (CB only: mean dorsal-ventral position of −177.1 ± 1.6μm; CB+CR: −145.7 ± 8.6μm; $P = 0.003$, Wilcoxon rank sum test). A similar distribution pattern is observed at P7 (CB only: −238.0 ± 2.7μm; CB+CR: −171.1 ± 17.5μm; $P < 0.001$, Wilcoxon rank sum test). Very few neurons coexpress CB and CR at P14 (Fig. 2E), but at P28 CB+CR neurons are not differentially located within the CB population (CB only: −287.1 ± 12.0μm; CB+CR: −325.5 ± 15.1μm; $P = 0.27$, Wilcoxon rank sum test).

In contrast, PV coexpression is primarily observed in the ventral domain of the CB-expressing population when PV expression in neurons is first observed at P7. The distribution is also significantly different from the calretinin-coexpressing population at this age (CB+PV: −292.4 ± 50.5μm; $P < 0.05$, Wilcoxon rank sum test). PV coexpression expands dorsally at P14 and P28, but the majority of CB+PV cells are found near the ventral gray-white border. At P7, P14, and P28, a subset of neurons that coexpress CB, CR, and PV was found in the ventral domain of the CB distribution and the mean position of this cluster was significantly distinct from the CB distribution at all three stages (CB+CR+PV: −328.4 ± 6.2μm at P7, −317.0 ± 2.9μm at P14; −325.5 ± 9.9μm at P28; $P \leq 0.01$ for all age comparisons, Wilcoxon rank sum test).

As a first step in identifying the type of information CB neurons may be involved in processing, we quantified the prevalence and distribution of CB neurons contacted by VGLUT1 puncta, a putative marker of primary sensory afferent synapses in the ventral spinal cord. High-magnification confocal images were analyzed to determine putative synaptic contacts on the soma and proximal dendrites of CB-expressing neurons (Fig. 5A). While many neurons express CB at P0, only a minority of these cells received one or more VGLUT1 puncta (Fig. 5B; 15.7 ± 6.9%, 77 cells analyzed from n = 3 animals). From P7, however, more than half of the analyzed CB-positive neurons received putative synaptic contacts from primary sensory afferents (Fig. 5B; P7: 56.4 ± 4.8%, 131 cells analyzed; P14: 66.1 ± 1.8%, 133 cells analyzed; P28: 62.3 ± 6.8%, 97 cells analyzed; 3 animals were analyzed at each age). Among the subset of neurons contacted by at least one VGLUT1 punctum, more than one-half (P7: 53.3%; P14: 65.1%: P28: 56.6%) were contacted by three or more putative synaptic contacts on the soma and proximal dendrites. In fact, some cells were covered by numerous VGLUT1 puncta (maximum number of putative contacts on a single CB neuron: 27 at P7, 26 at P14, 28 at P28). The average number of putative contacts was greatest at P14 (mean number of contacts: P7, 4.0 on 75 neurons; P14, 6.0 on 86 neurons; P28, 4.0 on 60 neurons). At P14, there was also greater variety in the numbers of putative contacts per neuron (Fig. 5C). This is evident when comparing the cumulative relative frequency distributions from P7, P14, and P28 animals where the distribution at P14 is significantly different from P7 and P28 (Kruskal-Wallis test $P < 0.005$; pairwise differences of average ranks tests: P7 vs. P14 and P28 vs. P14, $P < 0.0001$; P7 vs. P28, not significant).

Two defining features of Renshaw cells are expression of CB and cell body position close to the ventral gray-white matter boundary. While unequivocal identification of Renshaw cells requires additional morphological criteria, the subset of CB-expressing neurons found within 100um of the gray-white border are enriched for Renshaw cells (Alvarez et al., 2005; Mentis et al., 2006). Using this guideline, VGLUT1 puncta on this group of extreme ventral CB cells were analyzed separately. At P7 and P14, the profile of putative contacts observed on the extreme ventral subset was similar to that of the total CB-expressing population (Fig. 5C). In both populations, the number of putative contacts is most varied at P14. The putative contact distribution for extreme ventral CB neurons, however, is retracted at P28 compared with the overall population (Fig. 5C).

Discussion

Here we have quantified the changing CB expression pattern in the ventral spinal cord across postnatal development. Fewer neurons express CB as postnatal development progresses and those neurons frequently coexpress other calcium binding proteins (PV and CR) in subsets with distinct spatial distributions. A significant portion of CB-expressing neurons receive putative synaptic contacts from primary sensory afferents, and based on positional information, CB-expressing neurons in the ventral horn likely include subpopulations that are not Renshaw cells.

At P0, neurons expressing CB are distributed in a fairly uniform pattern throughout the ventral horn and are at least 5-fold more numerous than at P28. Reduced CB expression has been noted in adults, and the postnatal decline observed in this study is in general agreement with previous reports (Alvarez et al., 2005; Anelli and Heckman, 2005; Siembab et al., 2010; Zhang et al., 1990). The largest drop in expression occurs between P7 and P14 in our data. Significant milestones in locomotor development occur during the second postnatal week (Geisler et al., 1993). Perhaps most relevant to this study is the emergence of weight-bearing locomotion (Altman and Sudarshan, 1975). Efficient quadrupedal locomotion depends on locomotor circuits fully capable of integrating sensory feedback, and decreased prevalence of CB expression in the ventral horn may signify the maturation of these circuits. Expression of calretinin coincides with expression of markers of immature, adult-born neurons in the hippocampus, but is lost (or in some cases replaced by CB expression) as neurons mature (Brandt et al., 2003). Persistent CB expression in some ventral interneurons, including Renshaw cells, points to the need for precise Ca^{2+} regulation in the mature function of particular neurons. This expression may be influenced by neuronal activity. After disruption of both motor and sensory activity following a sciatic nerve lesion, CB expression in lumbar spinal cord Renshaw cells is reduced, but expression returns following motor reinnervation of target muscles (Sanna et al., 1993). This may not be a global response of Renshaw cells, however, as no changes in CB expression were reported in the cervical spinal cord after a similar injury (Fallah and Clowry, 1999). CB expression may be less influenced by the activity of primary sensory afferents and descending pathways. In mutant mouse models that lead to a selective increase or decrease in ventral horn primary sensory afferent synapses, the number of CB-expressing cells is unchanged (Siembab et al., 2016). Similarly, ablation of descending inputs to the lumbar spinal cord following neonatal thoracic cord transection, does not appear to reduce CB expression in ventral horn Renshaw cells (Smith et al., 2017).

The high incidence of coexpression of calretinin and/or parvalbumin in CB-expressing neurons with increasing age (>70% of CB neurons at P28) has not been previously reported. In fact, other than frequent coexpression in Renshaw cells, the consistent finding in other studies has been the absence of coexpression (Alvarez et al., 2005; Anelli and Heckman, 2005). Differences in species and age may contribute to the discrepancy. Anelli and Heckman studied the adult cat, while mice used by Alvarez and colleagues included both P18–P30 (ages overlapping with our study) and 3 month-old animal cohorts. Expression of additional calcium binding proteins may provide redundancy and increased buffering capacity.

CB neurons coexpressing PV were found concentrated along the ventral border beginning at P7 in the current study, similar to findings reported by Alvarez and colleagues (Alvarez et al., 2005). In addition, we identified a group of dorsally located neurons coexpressing CB and CR at P0 and P7. These spatially distinct subpopulations may be derived from different cell lineages. While Alvarez and colleagues determined CB neurons found within 100μm of the gray-white border in lamina VII are all V1 derived, only 50% of those found 100μm to 300μm from the gray-white border (upper dorsal lamina VII) were V1-derived (Alvarez et al., 2005). Heterogeneity in progenitor marker expression suggests not all CB-expressing interneurons in the ventral horn are V1-derived, but the present study does not provide direct evidence for dorsal CB- and CR-positive cells arising from a specific cell lineage.

In the spinal cord, VGLUT1 is enriched in the synaptic terminals of primary sensory afferents and corticospinal tract neurons (Alvarez et al., 2004; Du Beau et al., 2012; Hantman and Jessell, 2010; Todd et al., 2003). In the ventral spinal cord where we focused our analysis, synaptic terminals arising from corticospinal axons are rare, and the vast majority of VGLUT1 puncta mark synaptic boutons of muscle spindle primary sensory afferents (Alvarez et al., 2004; Du Beau et al., 2012; Oliveira et al., 2003).

While the number of CB-expressing neurons did not significantly change from P0 to P7, the fraction of these neurons receiving putative synaptic contacts increased from 15% to approximately 50%, indicating a period of sensory afferent synaptic proliferation within the ventral horn. The fraction of CB-expressing cells receiving contacts at P14 and P28 remained fairly stable, while the total number of CB-expressing cells was reduced at these time points compared to P0. This suggested similar proportions of connected and non-connected cells downregulated CB expression during this time.

While the level of connectivity for most cells was modest (1 to 4 putative contacts), some cells throughout the ventral cord were found to be heavily connected. The average number of putative contacts per cell peaks at P14 and decreases somewhat at P28. This pattern follows the general trend in previous reports of sensory afferent contacts on Renshaw cells, a subset of CB-expressing interneurons and the only CB cell type analyzed to date for primary sensory afferent contacts. Sensory-derived synaptic inputs on these cells proliferate postnatally up to P15, but are reduced later in development (Mentis et al., 2006).

Among identified interneuron populations in the spinal cord, the presence or absence of primary sensory afferent contacts is a useful criterion for drawing broad-brush distinctions

between genetically defined subsets of interneurons (Lu et al., 2015). While CB-expressing ventral interneurons may stem from multiple domains, the mixed status of primary sensory afferent connectivity among neurons linked by expression of this marker more strongly suggests a heterogeneous population. Future studies to investigate the efficacy of putative synaptic contacts on non-Renshaw cell, CB-positive interneurons may elucidate multiple functional identities within this group.

In summary, we have quantified the decrease in CB expression among ventral interneurons during postnatal development. Cells that continue to express CB may share commonalities in function or connectivity. We observed, however, significant heterogeneity among these neurons, with some coexpressing other calcium binding proteins, and a subset receiving putative synaptic inputs from primary sensory afferents. Derivation of CB neurons from multiple cell lineages may contribute to this heterogeneity. Characterization of primary sensory afferent contacts on CB-expressing cells from distinct ventral interneuron lineages could determine if cells categorized by this parameter align with specific lineages.

Experimental Procedures

Spinal Cord Tissue Preparation

All animal procedures were approved by the Wright State University Institutional Animal Care and Use Committee and carried out according to NIH guidelines. C57BL/6J mice were used in this study and tissue was collected within 24 hours of birth (designated postnatal day (P) 0), and at one, two, and four weeks postnatal (P7, P14, P28). Animals were deeply anesthetized and then transcardially perfused with 4% paraformaldehyde in 0.1M phosphate buffer (pH 7.4). After perfusion, the spinal cord was exposed via laminectomy and immersion fixed for 2 hours in 4% paraformaldehyde at 4°C. The tissue was transferred to a 30% sucrose solution (in PBS) for cryoprotection before freezing. Spinal cords were serial sectioned with a cryostat at a thickness of 20μm and mounted in sequence on four series of slides for immunostaining and quantification. Distributing serial sections across four series meant adjacent sections on the same slide were separated by 80μm along the rostral-caudal axis of the spinal cord. The average number of sections analyzed for CB expression and coexpression with CR and PV with this approach in each of the five animals at each time point were: P0, 24.8 ± 0.3; P7, 37.2 ± 1.7; P14, 56 ± 1.0; P28, 33.8 ± 1.0 (mean ± SEM).

Immunohistochemistry

Primary antibodies were diluted in a blocking buffer solution (1% bovine serum albumin and 0.1% Triton X-100 in PBS) and slides were incubated overnight at 4°C. Prior to primary antibody incubation to assess coexpression of calcium binding proteins, tissue from P14 and P28 animals was pre-treated for antigen retrieval with 10mM sodium citrate buffer solution (in PBS, pH 6.0) for 20 minutes at 95°C. Primary antibodies and working dilutions used in this study were: rabbit polyclonal anti-recombinant rat calbindin D-28k (1:1000, Swant, Marly, Switzerland; cat. no. CB-38a), goat polyclonal anti-parvalbumin (1:9000, Swant; cat. no.PVG-214), mouse monoclonal anti-full-length recombinant mouse calretinin protein (1:5000, Invitrogen, Camarillo, CA; cat. no. 18-0291), and guinea pig polyclonal anti-VGLUT1 (1:10,000, Chemicon; cat. no. AB5905). Antibody specificity has been previously

validated by the absence of specific staining on spinal cord sections from knockout mice (CB and VGLUT1; Siembab et al., 2016), lack of staining when pre-incubated together with purified recombinant proteins (PV; Xu et al., 2010), or cell-type specific staining patterns in mouse retina (CR; Du et al., 2015). All primary antibodies were revealed with appropriate fluorescent donkey anti-rabbit/goat/guinea pig/mouse secondary antibodies, incubated for 45 minutes at room temperature. Vectashield was used under coverslips to minimize fading (Vector Labs, Burlingame, CA).

Image Acquisition and Analysis

Slides were initially reviewed on an Olympus BX-51 epifluorescence microscope. Only one of the four series of slides was stained for quantification of CB expression. On each slide, all sections of the three lumbar domains (L1/L2, L3/L4, L5/L6) were analyzed to determine the number of CB-expressing neurons in the ventral spinal cord. Spatial analysis of CB coexpression with CR and PV was carried out in several stages using one of the four series of slides. First, brightfield images of the entire spinal cord section were acquired using a 10X objective to establish the outline of the cord using a CCD camera (RT Slider) controlled by Spot software (Diagnostics Instruments, Inc.). From these images, coordinates of key structures and boundaries of the spinal cord were digitized using ImageJ to enable alignment of data sets from multiple images within a lumbar domain in later analyses. These points included the central canal, and the ventral- and lateral-most boundaries of the cord. In this study, the ventral spinal cord is defined by a horizontal line extending laterally from the central canal. The images were also annotated with color-coded dots within the Spot software to indicate the location of CB and coexpressing cells. Colocalization was confirmed in selected sections by confocal microscopy using an Olympus FV1000 system.

Custom routines written in Matlab (The MathWorks, Natick, MA) were used to analyze the annotated images and combine data from multiple sections and all animals for each time point within each lumbar domain. For each image, x and y coordinates (in μm) of all labeled cells were assigned with respect to the central canal, which was identified as the origin (0,0). To combine data from multiple sections within the same lumbar domain, boundary coordinates obtained from brightfield images were averaged to construct a standardized outline of the cord. The set of x,y coordinates for cells in each image were then scaled to match the average spinal cord, thus creating a standardized, two-dimensional Cartesian space for each lumbar domain and time point. As no significant difference in CB-expressing distributions were observed between the left and right side of the spinal cord, data from both sides were combined into a single, hemi-cord coordinate system and data is plotted on the right side of the ventral cord.

To detect potential contacts from primary sensory afferents on CB-expressing neurons, confocal images were taken at high magnification (Olympus FV1000, 60X objective, 0.3μm z-step size). Determining the connectivity for all CB neurons in a given section was not practical, particularly at younger ages when calbindin expression is abundant. In order to sample the CB population in an unbiased manner, each side of the ventral spinal cord was divided into two halves along the medial-lateral axis, resulting in four regions (left-medial half, left-lateral half, right-medial half, right-lateral half). One of these four regions was

chosen at random for each section to be imaged, and if more than one CB-expressing neuron was found within that region, one cell was chosen at random to be imaged. Putative VGLUT1 synaptic contacts were identified through manual inspection of individual optical sections using Imaris software (version 8.0, Bitplane, Zurich). Close apposition of VGLUT1 and CB signals, with no visible gap between the two signals, was required in order to conclude a VGLUT1-positive sensory terminal was likely making contact with the CB-expressing neuron.

Statistical analysis and data visualization

Statistical analyses were performed using SPSS Statistics version 23 (IBM) and R. ANOVA followed by Tukey's HSD pairwise comparisons was used for analysis of CB expression in different lumbar domains across time (Fig. 1). Large variations in the number of coexpressing neurons at different time points violated key assumptions of ANOVA, therefore the Wilcoxon rank-sum test was used to compare distributions of cell types with different coexpression signatures along the dorsal-ventral axis (Fig. 4). Lastly, cumulative distributions of VGLUT1 puncta on CB-expressing neurons were analyzed by the Kruskal-Wallis test to determine group differences, followed by pairwise differences of average ranks tests for individual group comparisons. Quantitative data is presented as mean ± standard error of the mean (SEM).

Plots of CB distribution (Fig. 4) were produced using the "geom_boxplot" and "geom_density" functions in the ggplot2 library in R (Wickham, 2009). The "geom_density" function provides one-dimensional density estimation of the distribution probability and the integral of the curve sums to unity.

Acknowledgments

Grant Sponsor: NIH NINDS

Grant Number: NS072454

The authors declare no competing financial interests. The authors gratefully acknowledge Michael A. Bottomley and the Statistical Consulting Center at Wright State University for statistical advice and help with R. Likewise, the authors acknowledge Kerri Beedy, Phillip Cohen, Kristen Dorsey, Daniel Ross, Alexandra Shishoff, and Andrew Slusher for assistance with image analysis. YD receives support from the Biomedical Sciences PhD program at Wright State.

References

Altman J, Sudarshan K. Postnatal development of locomotion in the laboratory rat. Anim Behav. 1975; 23:896–920. [PubMed: 1200422]

Alvarez FJ, Fyffe REW. The continuing case for the Renshaw cell. J Physiol. 2007; 584:31–45. [PubMed: 17640932]

Alvarez FJ, Jonas PC, Sapir T, Hartley R, Berrocal MC, Geiman EJ, Todd AJ, Goulding M. Postnatal phenotype and localization of spinal cord V1 derived interneurons. J Comp Neurol. 2005; 493:177–192. [PubMed: 16255029]

Alvarez FJ, Villalba RM, Zerda R, Schneider SP. Vesicular glutamate transporters in the spinal cord, with special reference to sensory primary afferent synapses. J Comp Neurol. 2004; 472:257–80. [PubMed: 15065123]

Andressen C, Blümcke I, Celio MR. Calcium-binding proteins: selective markers of nerve cells. Cell Tissue Res. 1993; 271:181–208. [PubMed: 8453652]

Anelli R, Heckman CJ. The calcium binding proteins calbindin, parvalbumin, and calretinin have specific patterns of expression in the gray matter of cat spinal cord. J Neurocytol. 2005; 34:369–85. [PubMed: 16902759]

Arber S, Ladle DR, Lin JH, Frank E, Jessell TM. ETS gene Er81 controls the formation of functional connections between group Ia sensory afferents and motor neurons. Cell. 2000; 101:485–98. [PubMed: 10850491]

Arvidsson U, Ulfhake B, Cullheim S, Ramírez V, Shupliakov O, Hökfelt T. Distribution of calbindin D28k-like immunoreactivity (LI) in the monkey ventral horn: do Renshaw cells contain calbindin D28k-LI? J Neurosci. 1992; 12:718–28. [PubMed: 1545236]

Benito-Gonzalez A, Alvarez FJ. Renshaw cells and Ia inhibitory interneurons are generated at different times from p1 progenitors and differentiate shortly after exiting the cell cycle. J Neurosci. 2012; 32:1156–70. [PubMed: 22279202]

Bikoff JB, Gabitto MI, Rivard AF, Drobac E, Machado TA, Miri A, Brenner-Morton S, Famojure E, Diaz C, Alvarez FJ, Mentis GZ, Jessell TM. Spinal inhibitory interneuron diversity delineates variant motor microcircuits. Cell. 2016; 165:207–19. [PubMed: 26949184]

Brandt MD, Jessberger S, Steiner B, Kronenberg G, Reuter K, Bick-Sander A, von der Behrens W, Kempermann G. Transient calretinin expression defines early postmitotic step of neuronal differentiation in adult hippocampal neurogenesis of mice. Mol Cell Neurosci. 2003; 24:603–13. [PubMed: 14664811]

Brini M, Calì T, Ottolini D, Carafoli E. Neuronal calcium signaling: function and dysfunction. Cell Mol Life Sci. 2014; 71:2787–814. [PubMed: 24442513]

Carr PA, Alvarez FJ, Leman EA, Fyffe RE. Calbindin D28k expression in immunohistochemically identified Renshaw cells. Neuroreport. 1998; 9:2657–61. [PubMed: 9721951]

Du M, Otalora L, Martin AA, Moiseyev G, Vanlandingham P, Wang Q, Farjo R, Yeganeh A, Quiambao A, Farjo KM. Transgenic mice overexpressing Serum Retinol-Binding Protein develop progressive retinal degeneration through a retinoid-independent mechanism. Mol Cell Biol. 2015; 35:2771–89. [PubMed: 26055327]

Du Beau A, Shakya Shrestha S, Bannatyne BA, Jalicy SM, Linnen S, Maxwell DJ. Neurotransmitter phenotypes of descending systems in the rat lumbar spinal cord. Neuroscience. 2012; 227:67–79. [PubMed: 23018001]

Fallah Z, Clowry GJ. The effect of a peripheral nerve lesion on calbindin D28k immunoreactivity in the cervical ventral horn of developing and adult rats. Exp Neurol. 1999; 156:111–20. [PubMed: 10192782]

Fyffe RE. Evidence for separate morphological classes of Renshaw cells in the cat's spinal cord. Brain Res. 1990; 536:301–4. [PubMed: 2085756]

Geisler HC, Westerga J, Gramsbergen A. Development of posture in the rat. Acta Neurobiol Exp (Wars). 1993; 53:517–23. [PubMed: 8109261]

Hantman AW, Jessell TM. Clarke's column neurons as the focus of a corticospinal corollary circuit. Nat Neurosci. 2010; 13:1233–9. [PubMed: 20835249]

Kiehn O. Decoding the organization of spinal circuits that control locomotion. Nat Rev Neurosci. 2016; 17:224–38. [PubMed: 26935168]

Lu DC, Niu T, Alaynick WA. Molecular and cellular development of spinal cord locomotor circuitry. Front Mol Neurosci. 2015; 8:25. [PubMed: 26136656]

Mentis GZ, Siembab VC, Zerda R, O'Donovan MJ, Alvarez FJ. Primary afferent synapses on developing and adult Renshaw cells. J Neurosci. 2006; 26:13297–310. [PubMed: 17182780]

Oliveira ALR, Hydling F, Olsson E, Shi T, Edwards RH, Fujiyama F, Kaneko T, Hökfelt T, Cullheim S, Meister B. Cellular localization of three vesicular glutamate transporter mRNAs and proteins in rat spinal cord and dorsal root ganglia. Synapse. 2003; 50:117–29. [PubMed: 12923814]

Rexed B. The cytoarchitectonic organization of the spinal cord in the cat. J Comp Neurol. 1952; 96:414–95. [PubMed: 14946260]

Sanna PP, Celio MR, Bloom FE, Rende M. Presumptive Renshaw cells contain decreased calbindin during recovery from sciatic nerve lesions. Proc Natl Acad Sci U S A. 1993; 90:3048–52. [PubMed: 8464922]

Schwaller B. Cytosolic Ca2+ buffers. Cold Spring Harb Perspect Biol. 2010; 2:a004051. [PubMed: 20943758]

Siembab VC, Gomez-Perez L, Rotterman TM, Shneider NA, Alvarez FJ. Role of primary afferents in the developmental regulation of motor axon synapse numbers on Renshaw cells. J Comp Neurol. 2016; 524:1892–919. [PubMed: 26660356]

Siembab VC, Smith CA, Zagoraiou L, Berrocal MC, Mentis GZ, Alvarez FJ. Target selection of proprioceptive and motor axon synapses on neonatal V1-derived Ia inhibitory interneurons and Renshaw cells. J Comp Neurol. 2010; 518:4675–701. [PubMed: 20963823]

Smith CC, Paton JFR, Chakrabarty S, Ichiyama RM. Descending systems direct development of key spinal motor circuits. J Neurosci. 2017; 37:6372–87. [PubMed: 28576940]

Thomas RC, Wilson VJ. Precise localization of Renshaw cells with a new marking technique. Nature. 1965; 206:211–3.

Todd AJ, Hughes DI, Polgár E, Nagy GG, Mackie M, Ottersen OP, Maxwell DJ. The expression of vesicular glutamate transporters VGLUT1 and VGLUT2 in neurochemically defined axonal populations in the rat spinal cord with emphasis on the dorsal horn. Eur J Neurosci. 2003; 17:13–27. [PubMed: 12534965]

Watson, C., Paxinos, G., Kayalioglu, G., Heise, C. An atlas of the mouse spinal cord. In: Watson, C.Paxinos, G., Kayalioglu, G., editors. The Spinal Cord. A Christopher and Dana Reeve Foundation Text and Atlas. Elsevier Academic Press; San Diego: 2009. p. 308-379.

Wickham, H. ggplot2: Elegant Graphics for Data Analysis. Springer-Verlag; New York: 2009.

Xu X, Roby KD, Callaway EM. Immunochemical characterization of inhibitory mouse cortical neurons: three chemically distinct classes of inhibitory cells. J Comp Neurol. 2010; 518:389–404. [PubMed: 19950390]

Zhang JH, Morita Y, Hironaka T, Emson PC, Tohyama M. Ontological study of calbindin-D28k-like and parvalbumin-like immunoreactivities in rat spinal cord and dorsal root ganglia. J Comp Neurol. 1990; 302:715–28. [PubMed: 2081815]

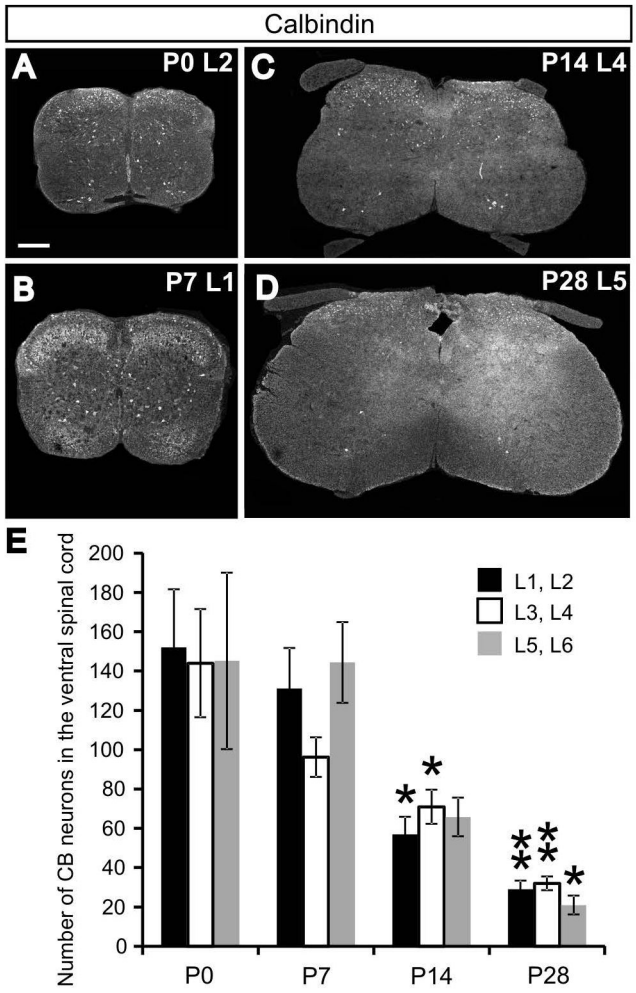

Fig. 1.

The number of neurons in the lumbar ventral spinal cord expressing calbindin (CB) decreases throughout postnatal development. **A–D:** Representative transverse sections at various lumbar spinal levels from P0–P28 illustrate a consistent decrease in CB expression in the ventral spinal cord (defined as the region ventral to the central canal). Scale bar in **A** applies to panels **A–D** and equals 200μm. **E:** Average numbers of CB-expressing neurons in three domains of the lumbar ventral cord at P0, P7, P14, and P28 time points. Numbers are derived from cell counts of every fourth serial section through the entire lumbar cord. Error bars indicate standard error of the mean (SEM), n=5 animals per age group. Asterisks indicate significant (* $P < 0.05$; ** $P < 0.01$; Tukey's HSD test) reductions in the number of expressing cells compared with P0 values within the same segments. Numbers of cells in the L1/L2 segments are significantly reduced compared to P0 values at both P14 and P28. This is the case for the L3/L4 segments, as well. The number of CB-expressing neurons in the L5/L6 domain is significantly reduced when compared to P0 values only at P28.

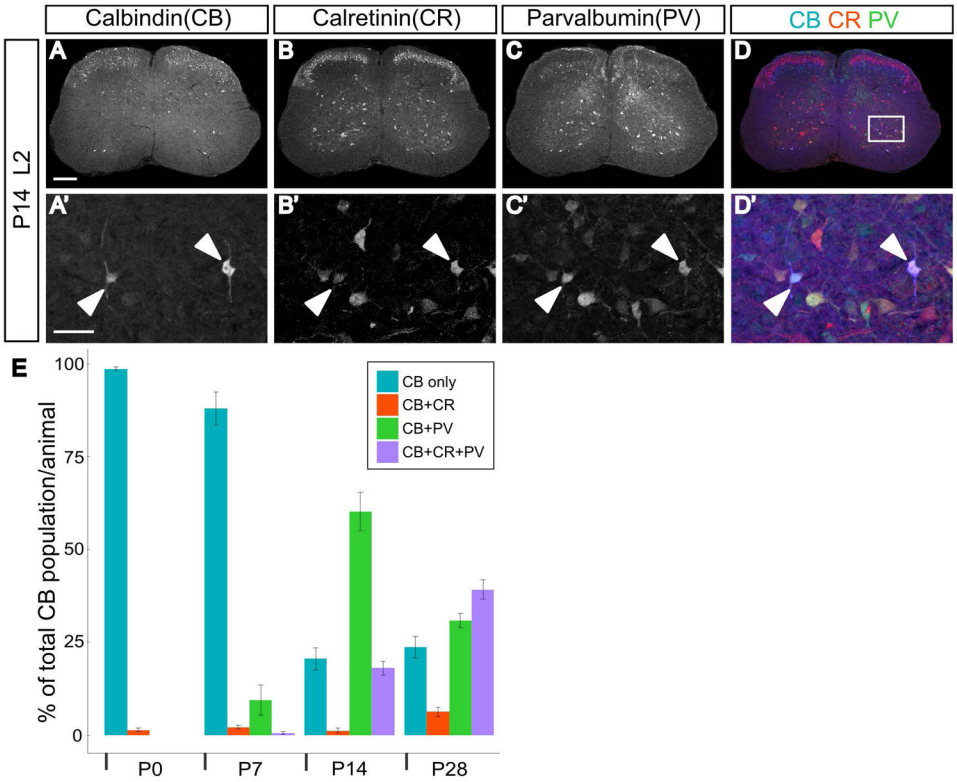

Fig. 2.

Coexpression of other calcium binding proteins in calbindin-expressing neurons increases during postnatal maturation. **A–D:** Representative transverse section from the L2 segment in a P14 animal showing expression of calbindin, calretinin, and parvalbumin. **A′–D′:** Enlarged view of region indicated by white box in **D**. Filled arrowheads point to CB, CR, and PV triple-positive cells. **A–D** scale bar=200μm and **A′–D′** scale bar=50μm. **E:** Percentage of calbindin-expressing neurons also expressing calretinin and/or parvalbumin during postnatal development. Error bars indicate standard error of the mean (SEM), n=5 animals per age group.

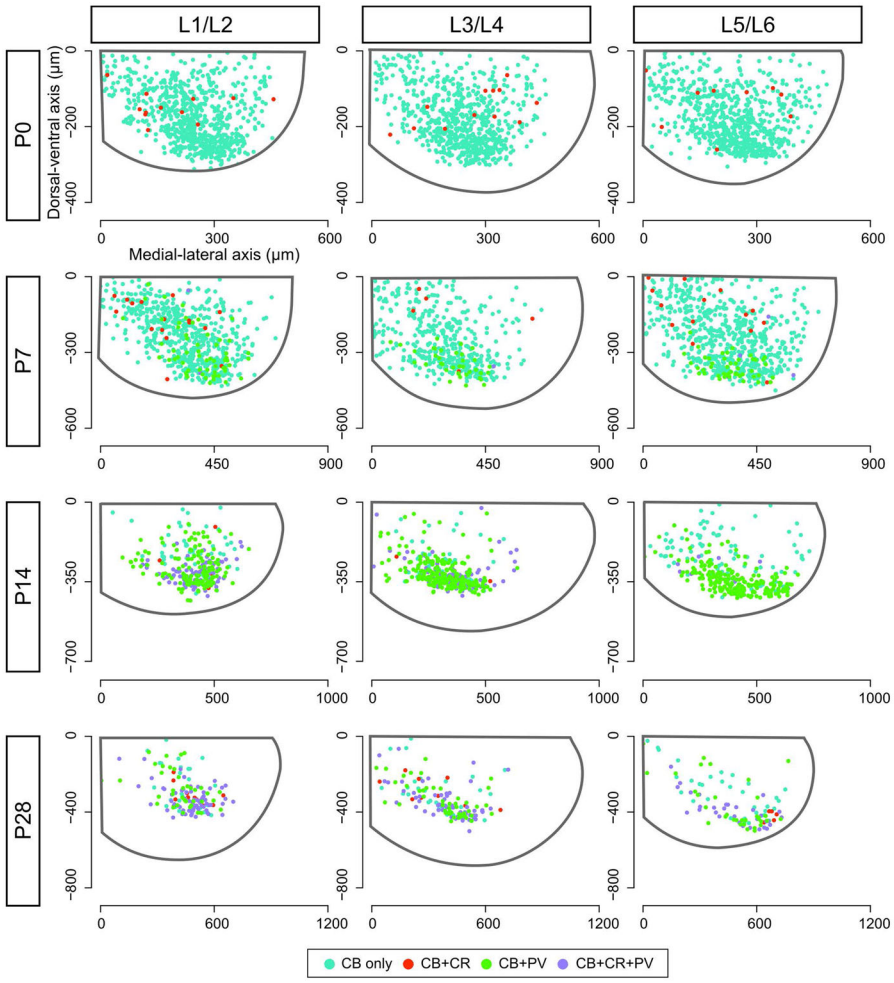

Fig. 3.

Expression pattern of calbindin and other coexpressed calcium binding proteins in the ventral spinal cord throughout development. Axes originate from the central canal (0, 0) and indicate distance from the origin (in μm) along the dorsal-ventral axis (ordinate) and medial-lateral axis (abscissa). Gray outline in each panel illustrates the outer border of the spinal cord derived from the average of all sections within a particular lumbar domain from 5 animals. Color-coded dots (key provided in figure) indicate positions of calbindin-expressing neurons standardized to match the average dimensions of the cord at that age. Cells observed on both the right and left sides of the spinal cord from all five animals at each time point are combined in this figure and plotted on a right-sided ventral hemi-cord.

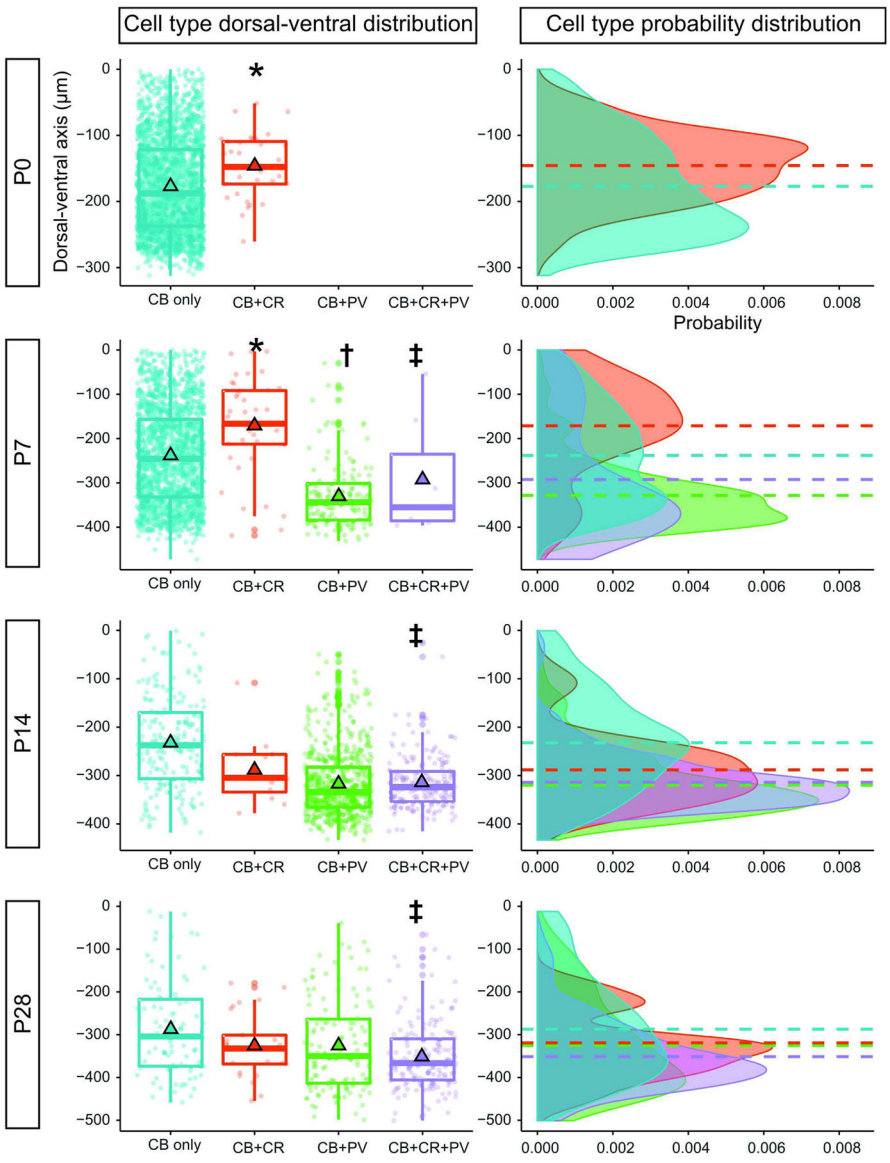

Fig. 4.

Spatial clustering of calbindin-expressing subtypes along the dorsal-ventral axis. **Left:** Box-and-whisker plots show the dorsal-ventral distribution of calbindin-expressing cells together with cells coexpressing other calcium binding proteins. Individual data points representing cells found throughout the lumbar cord in 5 animals of each age are overlaid on the box plot. The bottom, center, and top lines of each box denote the 25th, 50th (median), and 75th percentiles of the distribution, respectively. Mean values are represented by black-outlined triangles. Negative values along the dorsal-ventral axis indicate positions ventral to the central canal (defined as 0μm). Calbindin coexpression with parvalbumin (PV) was not detected at P0. Statistically significant pairwise comparisons are indicated with *(P <0.01; CB only vs. CB+CR), † (P <0.05; CB+CR vs. CB+PV), and ‡ (P <0.05; CB only vs. CB +CR+PV). **Right:** One-dimensional density estimate plots along the dorsal-ventral axis for each cell type. Probability distributions follow color schemes in left column. Dashed

horizontal lines indicate the mean position of each cell type along the dorsal-ventral axis and align with outlined triangles in the left column. The cumulative probability of each curve sums to unity. The relative probability of observing cells at different positions along the dorsal-ventral axis is represented on the abscissa.

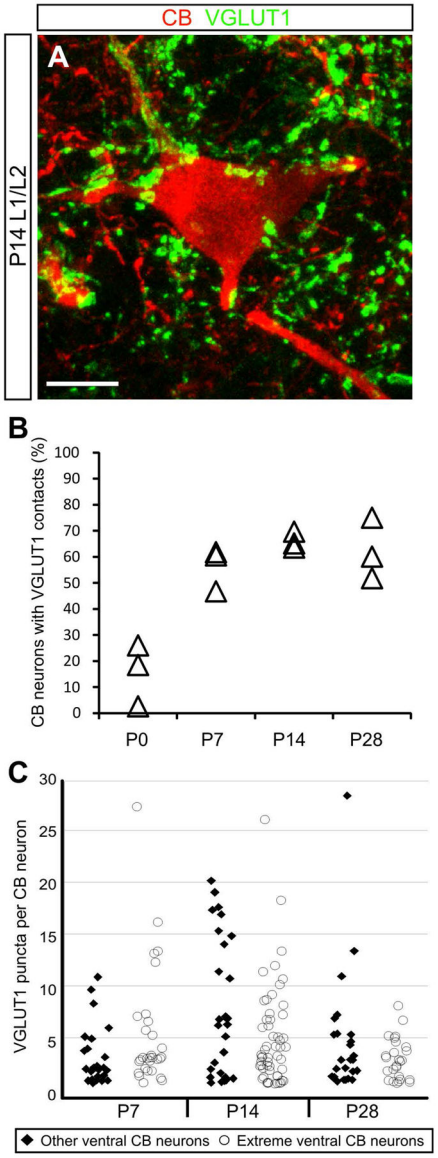

Fig. 5.

A subset of calbindin-expressing neurons receive putative synaptic contacts from primary sensory afferents. **A:** Representative image of a calbindin-expressing interneuron in the L1/L2 segment heavily contacted by VGLUT1 puncta, a putative marker of primary sensory afferent synapses. Image is a two-dimensional projection from a 24.3μm-thick confocal z-stack. Scale bar=10μm. **B:** Percent of analyzed calbindin neurons contacted by VGLUT1 puncta over postnatal development. The percent of all calbindin neurons receiving putative synaptic contacts are shown for three animals at each time point. **C:** Analyzed calbindin-expressing neurons were divided into two categories based on cell position: those found less than 100μm from the gray-white border in the ventral horn (extreme ventral CB neurons, open circles), and those whose position was greater than 100μm from the gray-white border

(other ventral CB neurons, filled diamonds). Pooled data from three animals analyzed at each time point are plotted in **C**.